


# Characterization of a 100 micrometer-scale cryogenically cooled gas jet for near-critical density laser-plasma experiments

Cite as: Rev. Sci. Instrum. **90**, 103001 (2019); <https://doi.org/10.1063/1.5109033>

Submitted: 05 May 2019 . Accepted: 04 September 2019 . Published Online: 04 October 2019

F. Salehi, A. J. Goers, L. Feder, B. Miao, D. Woodbury , and H. M. Milchberg



View Online



Export Citation



CrossMark

## ARTICLES YOU MAY BE INTERESTED IN

[A simple atomic beam oven with a metal thermal break](#)

Review of Scientific Instruments **90**, 053106 (2019); <https://doi.org/10.1063/1.5067306>

[An integrated instrument of DUV-IR photoionization mass spectrometry and spectroscopy for neutral clusters](#)

Review of Scientific Instruments **90**, 073101 (2019); <https://doi.org/10.1063/1.5108994>

[Femtosecond real-time probing of the excited-state intramolecular proton transfer reaction in methyl salicylate](#)

The Journal of Chemical Physics **151**, 094302 (2019); <https://doi.org/10.1063/1.5115307>



**MCL**  
MAD CITY LABS INC.

AFM & NSOM      Nanopositioning Systems      Micropositioning      Single Molecule Microscopes

# Characterization of a 100 micrometer-scale cryogenically cooled gas jet for near-critical density laser-plasma experiments

Cite as: Rev. Sci. Instrum. 90, 103001 (2019); doi: 10.1063/1.5109033

Submitted: 5 May 2019 • Accepted: 4 September 2019 •

Published Online: 4 October 2019



View Online



Export Citation



CrossMark

F. Salehi, A. J. Goers, L. Feder, B. Miao, D. Woodbury,  and H. M. Milchberg

## AFFILIATIONS

Institute for Research in Electronics and Applied Physics, University of Maryland, College Park, Maryland 20742, USA

## ABSTRACT

We present the design and characterization of a thin, high density pulsed gas jet for use in the study of near critical laser plasma interactions with ultrashort Ti:sapphire laser pulses. The gas jet uses a range of capillary nozzles with inner diameters between 50 and 150  $\mu\text{m}$  and is operated in the sonic regime. Cryogenic cooling of the gas valve body to  $-160^\circ\text{C}$  provides the necessary density enhancement for reaching overcritical plasma densities at  $\lambda = 800\text{ nm}$  ( $N_{cr} \approx 1.7 \times 10^{21}\text{ cm}^{-3}$ ) using hydrogen gas at jet backing pressures below 1000 psi. Under certain conditions, fast expansion of the gas from a nozzle can lead to formation of clusters; here, we use our previously demonstrated all-optical method to estimate the cluster mean size and density. For the jets studied here, we find that cluster formation only begins at distances from the nozzle exit greater than a few times the nozzle orifice diameter.

Published under license by AIP Publishing. <https://doi.org/10.1063/1.5109033>

## I. INTRODUCTION

Gas jets have been employed as targets in high intensity laser-matter interaction studies for decades. These experiments span a wide variety of applications including electron and ion acceleration,<sup>1–4</sup> high harmonic generation,<sup>5,6</sup> x-ray lasers,<sup>7</sup> and even generation of fusion neutrons.<sup>8</sup> The main advantages of gas jets, compared to thin foil solid targets or static gas fills, are that they are a well-controlled, automatically replenishing target that can be used at high laser pulse repetition rates without requiring target rasterization schemes, and they allow the laser to propagate through vacuum before reaching the interaction volume. Fine control of the gas density and profile has been demonstrated by multiple groups through engineering of the valve design,<sup>9–11</sup> nozzle geometry,<sup>12–15</sup> and through external shaping of the resulting gas flow.<sup>16–19</sup>

In prior experiments with gas jets, the gas density has generally been limited to less than  $\sim 10^{20}\text{ cm}^{-3}$ , with interaction lengths on the millimeter scale. For typical hydrogen or helium gas jets, this density limitation precludes the study of near critical laser plasma interactions using Ti:sapphire laser systems ( $\lambda = 800\text{ nm}$ , critical density  $N_{cr} \approx 1.7 \times 10^{21}\text{ cm}^{-3}$ ), which is of interest for laser driven electron<sup>4,20</sup> and ion<sup>21,22</sup> acceleration experiments. Two notable exceptions to this limitation are the schemes presented by Sylla *et al.*<sup>10</sup> and Kaganovich

*et al.*<sup>16</sup> for achieving thin, high density plasmas suitable for the study of near critical phenomena. Sylla *et al.* achieved a critical density plasma by implementing a novel valve design, which boosts the pressure above 4000 psi behind a 400  $\mu\text{m}$  nozzle. Kaganovich *et al.* generated a shockwave in a standard gas jet by ablating a nearby metal surface with a nanosecond laser pulse a controlled time before arrival of the main interacting pulse. The density in the thin shock can be many times higher than the ambient gas density, boosting the target density into the near critical regime.

Here, we present a method for generating thin, near critical density plasmas, which avoids pressure boosting schemes or secondary lasers. The technique uses a cryogenically cooled high pressure solenoid valve coupled to a variety of thin nozzles with inner diameter as small as 50  $\mu\text{m}$ . Cryogenic cooling increases the density of atoms or molecules inside the gas valve reservoir for a fixed valve backing pressure, which, in turn, increases the gas density at the nozzle exit plane. The jet can be operated in pulsed or continuous flow modes. Because near-critical plasma densities significantly reduce the threshold for relativistic self-focusing, this method of high density jet generation has made possible our recent results in accelerating meV-scale electron bunches using peak laser powers well below 1 TW at high repetition rates, currently up to 1 kHz.<sup>20,23,24</sup>

We note that in recent years, liquid jets, from flowing liquids or cryogenically cooled gases through microscale nozzles, have been used as nearly debris-free and renewable targets suitable for high repetition rate laser-plasma interactions<sup>25,26</sup> at well above critical density (for near infrared lasers). The flow velocity of these jets is typically high enough to support a  $\geq$ kHz repetition rate.<sup>26</sup> The use of liquid jet targets has led to electron acceleration to mega-electronvolt energies at kilohertz repetition rate (in the direction opposite to the laser propagation);<sup>27</sup> given the high density and sharp boundaries of the liquid jets, these targets, as well as solid hydrogen extrusion targets, have been employed for laser-driven proton acceleration.<sup>28–31</sup>

## II. HIGH DENSITY VALVE DESIGN

The high density jet design consists of a homemade nozzle and a high speed solenoid valve (Parker series 99 miniature valve) controlled through a commercial valve driver (Parker Iota One). The solenoid valve and the high pressure gas feed tube are held in a custom cooling jacket, which uses a combination of liquid nitrogen and electrically driven heating elements to control the valve reservoir temperature. The reservoir temperature can be controlled to within 1 °C between room temperature and –160 °C.<sup>32</sup> The valve seal is formed by a Teflon poppet on a 1 mm diameter orifice. The valve body is modified for mounting of a 3 mm thick adaptor plate. The poppet seat orifice transitions directly to a straight 1 cm long stainless steel capillary (the “needle nozzle”) with inner diameter ranging from 50  $\mu$ m to 150  $\mu$ m soldered to the adaptor plate. The needle nozzle length is set by accessibility of small  $f$ -number laser focusing in our laser interaction experiments. Upon opening of the poppet, the gas is forced through the needle nozzle into the vacuum chamber. The volume of the gas exiting the nozzle is negligible compared to the volume in the valve and feed tube, where the gas is effectively under stagnation conditions. As is well known, the nozzle shape has a significant effect on the gas density profile.<sup>33</sup> As discussed below, our use of straight nozzles and sonic flow give different profiles than supersonic nozzles employing a converging-diverging design to achieve high Mach number flows.<sup>9,34–36</sup>

Controlling the reservoir temperature  $T_0$  and pressure  $P_0$ , along with the nozzle diameter, enabled access to peak molecular densities in the range  $10^{19}$ – $10^{21}$  cm<sup>–3</sup> while maintaining a  $\sim$ 200  $\mu$ m target thickness. The radial density profile of the gas flow was nearly Gaussian with full width at half maximum (FWHM) of 150–250  $\mu$ m at a height 150  $\mu$ m above the nozzle orifice, depending on the nozzle inner diameter. Depending on the gas species used, when ionized this covers underdense through overdense plasma regimes for an  $\lambda = 800$  nm Ti:sapphire laser ( $N_{crit} \approx 1.7 \times 10^{21}$  cm<sup>–3</sup>).

The flow of gas from the jet can be modeled as the steady, one-dimensional isentropic flow of an ideal gas into a low pressure reservoir.<sup>37</sup> Gas from the reservoir is forced through the needle nozzle by the pressure gradient between the reservoir and vacuum chamber, which is held at a pressure  $P_b \sim 10$  mTorr. In an ideal 1D isentropic flow, the gas density  $N$  can be expressed in terms of the gas specific heat ratio,  $\gamma = \frac{C_p}{C_v} > 1$  and the local Mach number,  $M = v/c_s$  where  $v$  is the gas velocity,  $c_s$  is the sound speed, and  $N_0$  is the gas density at the reservoir,<sup>38</sup>

$$N = N_0 \left( 1 + \frac{\gamma - 1}{2} M^2 \right)^{-\frac{1}{\gamma - 1}}. \quad (1)$$

Equation (1) indicates the gas density drops rapidly as the Mach number increases [ $(\gamma - 1)^{-1} = 2.5$ , using  $\gamma = 1.4$  for H<sub>2</sub>]. Therefore, to reach the highest density possible at the nozzle exit, the Mach number should be minimized. This is in contrast to supersonic nozzles used for laser-plasma interaction experiments where a flat top transverse density profile is desirable. For both sonic and supersonic nozzles, the mass flow rate and the peak density are limited by sonic choking, which limits the flow velocity to  $M = 1$  at the minimum orifice diameter.<sup>38</sup>

For an ideal diatomic gas ( $\gamma = 1.4$ ) under 1D isentropic flow conditions, the molecular density at the choke point ( $M = 1$ ) is

$$N^* = N_0 \left( \frac{2}{\gamma + 1} \right)^{\frac{1}{\gamma - 1}} \cong 0.63 N_0 = 0.63 \frac{P_0}{k_b T_0}. \quad (2)$$

Equation (2) shows that increasing the gas density at the nozzle exit is achieved simply by increasing the gas density in the reservoir. Increasing the reservoir density is achieved by increasing the backing pressure  $P_0$  and decreasing the reservoir temperature  $T_0$ . Cryogenic cooling of the reservoir thus serves to increase the jet output density proportional to  $T_0^{-1}$  for fixed backing pressure. It should be noted that this relation holds regardless of the sonic ( $M = 1$ ) vs supersonic ( $M > 1$ ) nature of the nozzle, so cryogenic cooling is an effective method for increasing the density of supersonic nozzles such as those in Refs. 9, 10, and 34.

## III. EXPERIMENTAL SETUP

The output density of the gas jet as a function of temperature, pressure, and nozzle geometry was characterized by transverse interferometry with a 70 fs, 400 nm probe pulse derived from our 25 TW Ti:sapphire laser system.<sup>39,40</sup> Figure 1 shows a diagram of the experimental setup. The probe pulse passes through the gas jet and enters folded wave front interferometer, with the phase shift  $\Delta\phi(x, z)$  extracted using Fourier techniques,<sup>41</sup> where  $x$  is the coordinate transverse to the gas jet flow direction and  $z$  is the distance from the jet orifice along the flow. The extracted 2D phase profile is related to the radial refractive index profile  $n(r, z)$  through the inverse Abel transform

$$n(r, z) - 1 = -\frac{1}{k\pi} \int_r^{r_0} \left( \frac{d\Delta\phi(x, z)}{dx} \right) \frac{dx}{\sqrt{x^2 - r^2}}, \quad (3)$$

giving the gas density profile

$$N(r, z) = \frac{n(r, z) - 1}{2\pi\alpha}.$$

Here,  $k = 2\pi/\lambda$  is the probe wavenumber,  $r$  is the radial coordinate,  $r_0$  is a radius at which the gas density goes to zero, and  $\alpha$  is the gas molecular polarizability [ $\alpha(\text{H}_2) \cong 0.67 \times 10^{-24}$  cm<sup>3</sup> and  $\alpha(\text{He}) \cong 0.20 \times 10^{-24}$  cm<sup>3</sup>].<sup>42</sup> The integral transform of Eq. (3) can be solved numerically or analytically with a suitable analytic profile fit to  $\Delta\phi(x, z)$ .

In all measurements,  $\Delta\phi(x, z = z_0)$  was well fit by a Gaussian function at heights  $z_0 = 50$   $\mu$ m or more above the nozzle orifice. Taking  $\Delta\phi(x, z_0) = \Delta\phi_0 \exp\left(-\frac{x^2}{\sigma^2}\right)$ , the index profile is calculated from Eq. (3) to be

$$n(r, z_0) - 1 = \frac{1}{k} \frac{\Delta\phi_0}{\sqrt{\pi}\sigma} \exp\left(-\frac{r^2}{\sigma^2}\right).$$

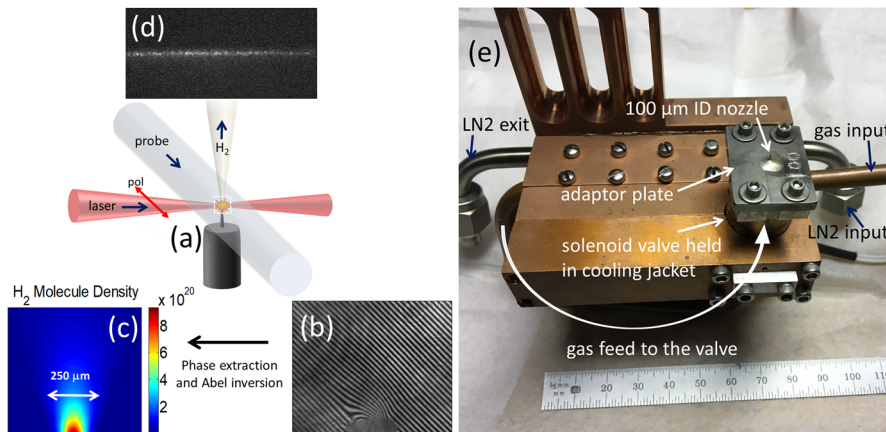


**FIG. 1.** Experimental setup for characterizing the high density gas jet (a). Density measurements were made using transverse interferometry. A raw interferogram (b) and Abel inverted density profile (c) are shown along with a raw image of Rayleigh scattering (d) used to measure the cluster size and density in the jet. Picture of the setup (e) shows the liquid nitrogen and gas feed tubes, and the solenoid valve held by the cooling jacket. The nozzle is mounted on the valve head via the adaptor plate.

A numerical Abel inversion routine based on the fast Fourier transform was also implemented.<sup>43</sup> Numerical Abel inversion generally agreed with the Gaussian fit-based analytical Abel inversion to within  $\sim 10\%$ . The panels in Fig. 1 depict a sample raw interferogram (b), Abel inverted density profile  $N(r, z)$  (c), a sample image of Rayleigh scattering (d) used to measure cluster size in the high density jet (see Sec. V), and a picture of the setup (e) showing the liquid nitrogen and the gas feed tubes, as well as the solenoid valve held by the cooling jacket. The adaptor plate, with the needle nozzle, is mounted on the valve head.

#### IV. HYDROGEN JET DENSITY MEASUREMENTS

Hydrogen gas is commonly used in laser plasma interaction experiments because of the ease with which it is fully ionized by the

leading temporal edge of a suitably intense femtosecond laser pulse. Complete ionization mitigates ionization-induced refraction of the main interacting pulse. However, since each hydrogen molecule can only contribute two electrons, high plasma densities have been very difficult to reach without the use of some higher Z gas such as nitrogen or argon. Figure 2(a) shows a sample Abel-inverted density profile  $N(r, z)$  of the hydrogen gas jet (100  $\mu\text{m}$  needle nozzle, 1000 psi backing pressure, and  $-160^\circ\text{C}$  reservoir temperature). The lineouts in Fig. 2(b), taken 70, 100, and 200  $\mu\text{m}$  above the nozzle, show a near-Gaussian radial density profile. The peak molecule density 70  $\mu\text{m}$  above the nozzle is  $9 \times 10^{20} \text{ cm}^{-3}$ , which, when fully ionized, gives a peak plasma density of  $1.8 \times 10^{21} \text{ cm}^{-3}$  or  $1.03 \times N_{crit}$  for  $\lambda = 800 \text{ nm}$ . Figure 2(c) shows the exponential decay of the peak gas density as a function of height above the nozzle for a series of backing pressures. The decay length is approximately 67  $\mu\text{m}$ ,

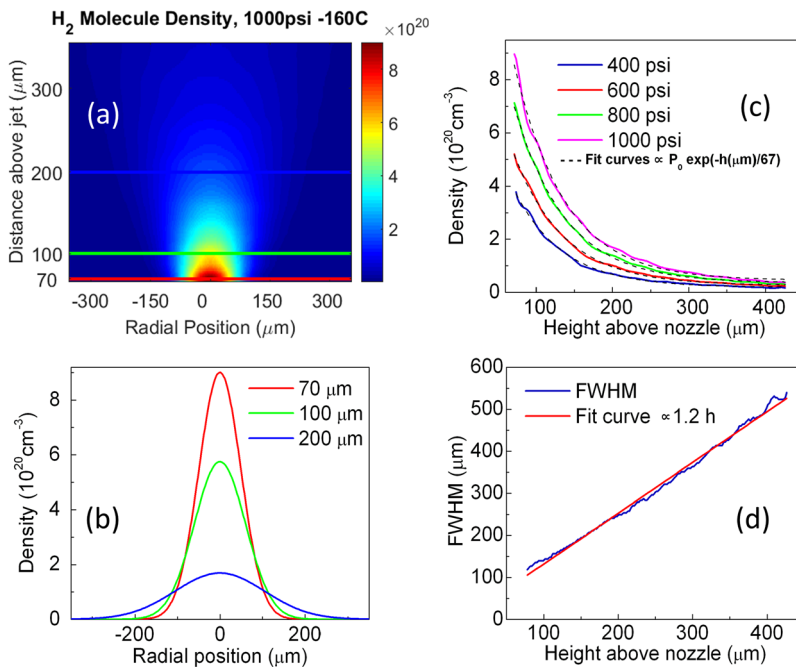


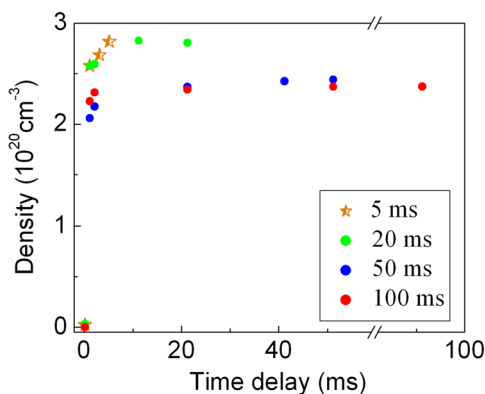
**FIG. 2.** Sample 2D hydrogen molecule density profile (a) with 1000 psi backing pressure and  $-160^\circ\text{C}$  reservoir temperature and lineouts 70, 100, and 200  $\mu\text{m}$  above the nozzle (b). The peak density as a function of height decays exponentially (c), and the FWHM increases linearly with height above the jet (d).

independent of the valve backing pressure. The exponential decay of the peak density is driven by the gas expansion, and the profile FWHM increases linearly as a function of height above the nozzle, as shown in Fig. 2(d).

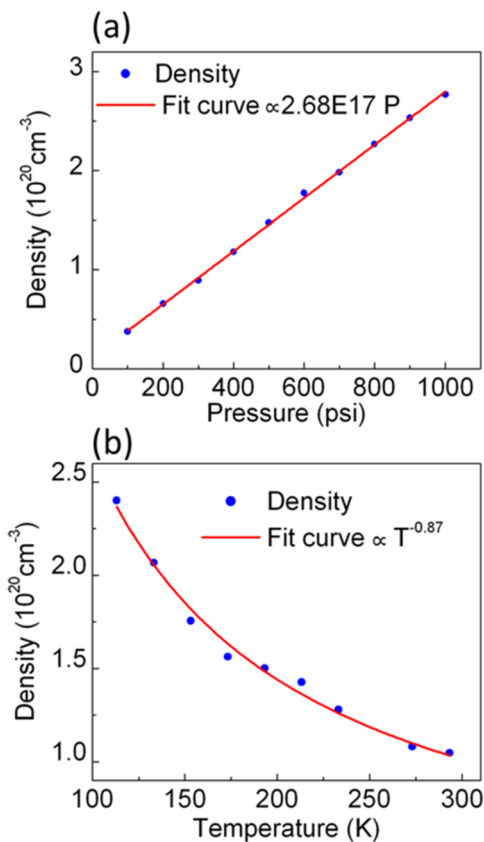
To minimize gas loading of the experimental chamber, the solenoid valve should have a fast rise time, reaching the desired stable output quickly. Figure 3 shows the measured temporal evolution of the helium gas output from a 150  $\mu\text{m}$  diameter needle nozzle with the valve reservoir held at 1100 psi and  $-140^\circ\text{C}$  for four different durations of the solenoid current pulse that drives the valve poppet. Each point in Fig. 3 represents the maximum measured gas density at 200  $\mu\text{m}$  above the needle nozzle. The 10%–90% rise time of the gas density is approximately 400  $\mu\text{s}$ , after which the measured output stabilizes for all four current pulse durations. The rise time was found to be relatively independent of pressure, temperature, and gas species. To minimize gas load, a current pulse duration of 700  $\mu\text{s}$  was used for all subsequent results in this paper. For high repetition rate applications, such as in our recent demonstration of mega-electronvolt electron acceleration at 1 kHz repetition rate, the current pulse can be set at arbitrarily long durations.<sup>23</sup> Also where the gas load is not an issue, it is possible to switch to continuous flow mode by removing the poppet.

Figure 4(a) shows the peak hydrogen molecule density 200  $\mu\text{m}$  above the 150  $\mu\text{m}$  diameter needle nozzle as a function of backing pressure with a fixed temperature of  $-160^\circ\text{C}$ . In agreement with the isentropic flow model, the measured density varies linearly with pressure. Figure 4(b) shows the dependence of the peak gas density at the same location for a fixed pressure of 1000 psi as a function of temperature. The peak density at  $-160^\circ\text{C}$  is enhanced by a factor of  $\sim 2.4$  compared to the peak density at room temperature, highlighting the effectiveness of cryogenic cooling for increasing gas jet density output. The measured density as a function of temperature is roughly proportional to  $T_0^{-0.87}$ . Departure from the  $1/T_0$  dependence is possibly caused by viscous effects in the flow, as the dynamic fluid viscosity is a function of the fluid temperature.<sup>44</sup>

Finally, the density of hydrogen gas was measured for a series of nozzles with inner diameters of 50, 100, and 150  $\mu\text{m}$ . Viscous forces cause significant pressure drop and therefore lower peak densities



**FIG. 3.** Helium density vs time delay at 200  $\mu\text{m}$  above the 150  $\mu\text{m}$  nozzle with the jet reservoir held at 1100 psi and  $-140^\circ\text{C}$  for 5 ms, 20 ms, 50 ms, and 100 ms current pulse durations.



**FIG. 4.** Peak hydrogen molecule density 200  $\mu\text{m}$  above the 150  $\mu\text{m}$  needle nozzle as a function of valve backing pressure at a fixed reservoir temperature  $-160^\circ\text{C}$  (113 K) (a) and as a function of reservoir temperature at a fixed backing pressure 1000 psi (b).

for smaller diameter nozzles. For all nozzle diameters, the peak density drops exponentially and the FWHM of the gas profile in the transverse direction increases linearly with height above the nozzle. Figure 5 shows the output density as a function of height for a fixed reservoir temperature and pressure of  $-160^\circ\text{C}$  and 1000 psi for all three nozzle diameters.

## V. CLUSTER SIZE AND DENSITY MEASUREMENTS

In many experiments involving high pressure gas jets, clustering of molecules can play an important role. Collisional ionization within the solid density clusters can greatly enhance ionization and increase laser-plasma coupling.<sup>45,46</sup> The laser cluster interaction has been demonstrated as a source of fast ions,<sup>2,47</sup> electrons,<sup>48,49</sup> x-rays,<sup>46,50</sup> and even neutrons.<sup>8,51</sup> Ballistic cluster flows can also be used to make shaped plasma density profiles using obstructions smaller than the cluster mean free path.<sup>19</sup>

The mean size and density of clusters in the high density gas jet can be estimated through an all optical technique combining transverse interferometry and collection of Rayleigh scattered light from the clusters.<sup>40</sup> The Rayleigh scattered energy into a collection lens by

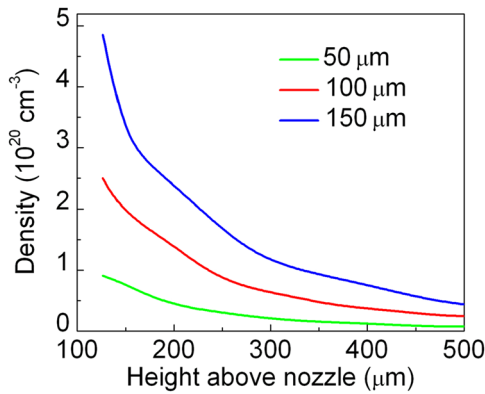


**FIG. 5.** Hydrogen molecule density as a function of height above needle nozzles with 50  $\mu\text{m}$  (green), 100  $\mu\text{m}$  (red), and 150  $\mu\text{m}$  (blue) inner diameter, all at  $-160^\circ\text{C}$  and 1000 psi.

a laser propagating from point  $x$  to  $x + \Delta x$  through a cluster jet is given by  $\Delta E_{lens}(x) \approx E_{in} \bar{\sigma}_{lens}(x) N_c(x) \Delta x$ , where  $E_{in}$  is the incident laser energy on the scattering volume,  $\bar{\sigma}_{lens}$  is the cross section for scattering into the lens averaged over the cluster size distribution, and  $N_c$  is the average cluster density. For  $90^\circ$  scattering and cluster sizes much less than the laser wavelength  $\sigma_{lens} = \pi k^4 |\Gamma|^2 (\alpha^2 - \alpha^4/4)$ , where  $k = 2\pi/\lambda$  is the laser wavenumber,  $\Gamma = a^3(\epsilon - 1)(\epsilon + 2)^{-1}$  is the cluster polarizability assuming a spherical cluster of radius  $a$  and dielectric constant  $\epsilon$ , and  $\alpha$  is the collection half angle of the imaging lens.<sup>40</sup> Using this cross section in the equation for the scattered energy gives

$$\bar{a}^6 N_c = \frac{1}{\pi k^4} \left| \frac{\epsilon + 2}{\epsilon - 1} \right|^2 \frac{\Delta E_{lens}}{E_{in} \Delta x} \left( \frac{1}{\alpha^2 - \alpha^4/4} \right), \quad (4)$$

where  $\bar{a}^6$  is an average of  $a^6$  over the cluster size distribution.<sup>40</sup> Transverse interferometry allows measurements of the real part of the refractive index  $n_r(x) = 1 + 2\pi N_c \Gamma_r$ , where  $\Gamma_r = \text{Re}(\Gamma)$ . Rearranging gives

$$\bar{a}^3 N_c = \frac{n_r(x) - 1}{2\pi} \left( \frac{\epsilon + 2}{\epsilon - 1} \right). \quad (5)$$

Combining Eqs. (4) and (5) yields an effective cluster radius  $a_{eff} \equiv (\bar{a}^6/\bar{a}^3)^{1/3}$  and number density  $N_{c,eff} \equiv \bar{a}^3 N_c/a_{eff}^3$ .<sup>40</sup>

The above model assumes complete clustering. If the jet contains a monomer fraction  $\delta_m = N_m/(N_m + N_c \bar{n}_c)$ , where  $N_m$  is the monomer density and  $\bar{n}_c$  is the average number of atoms in the cluster, the assumption of complete clustering causes an underestimation of  $a_{eff}$  by a factor  $(1 - \delta_m)^{-1/3}$ .<sup>40</sup> The underestimation arises from the additional contribution of the monomers to the measured phase shift while contributing negligibly to the Rayleigh scattered signal. The cube root dependence greatly reduces the effect of the uncertainty in  $\delta_m$  since even an assumption of 95% monomers only increases the calculated  $a_{eff}$  by a factor of 2.7. Furthermore, the effect of the cluster size distribution on  $a_{eff}$  can be calculated by comparing  $a_{eff} \equiv (\bar{a}^6/\bar{a}^3)^{1/3}$  to  $\bar{a}$  for various cluster size distributions,  $f(a)$ ,

where  $\bar{a}^n = \int_0^\infty a^n f(n_c) dn_c$  and  $a = r_{WS} n_c^{1/3}$  with  $r_{WS}$  the intra-cluster Wigner-Seitz radius. Using a log normal distribution for the number of molecules per cluster, we find that this method will tend to overestimate the cluster size. However, if the distribution is sufficiently narrow that the standard deviation is within 40% of the mean, then the retrieved cluster size,  $a_{eff}$ , will be correct to within a factor of 2.

Rayleigh scattering is collected from the cluster jet by focusing a 25 mJ,  $\sim 10$  ns (pulse duration set by unseeded regenerative amplifier) beam derived from our Ti:sapphire system ( $\lambda = 800$  nm) into the thin jet at  $f/9.5$ . A calibrated imaging system collects the scattered signal in a plane perpendicular to the pump polarization and images the signal onto a CCD camera. The experimental setup and a raw image of the Rayleigh scattered light are shown in Fig. 1. The same transverse interferometry diagnostic described in Sec. III was used to measure the clustered gas refractive index.

The hydrogen cluster size and density is found to vary as a function of the beam height above the nozzle orifice. Near the orifice, where the hydrogen molecule density is highest, negligible

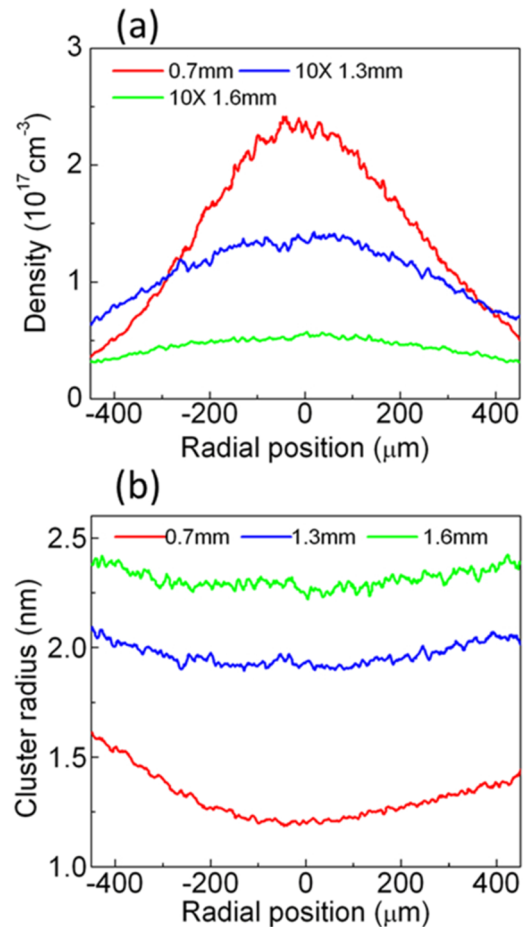


**FIG. 6.** Average cluster density (a) and average cluster size (b) as a function of radial position at various heights above the 150  $\mu\text{m}$  diameter nozzle orifice at jet backing pressure and temperature 1000 psi and  $-160^\circ\text{C}$ .

Rayleigh scattering was detected. A stronger Rayleigh scatter signal was observed farther from the nozzle, consistent with cooling-induced clustering as the gas expands into vacuum. Figure 6 shows the cluster size and density as a function of radial position at various heights above the 150  $\mu\text{m}$  diameter nozzle with a jet backing pressure of 1000 psi and reservoir temperature  $-160^\circ\text{C}$ . The minimum average cluster radius measured for any conditions was approximately 0.5 nm limited by the sensitivity of the Rayleigh scatter diagnostic.

At positions greater than approximately 500  $\mu\text{m}$  above the orifice, the cluster size is measurable and the dependence of clustering on jet backing pressure and reservoir temperature can be determined. Figure 7(a) shows the nonlinear dependence of the spatially integrated Rayleigh scatter signal on jet backing pressure at a height 1 mm above the 150  $\mu\text{m}$  nozzle when the jet reservoir temperature is held at  $-160^\circ\text{C}$ . Figure 7(b) shows the cluster size (dotted line) and density (solid line) at the same position as a function of backing pressure. The effective cluster radius dropped rapidly as the valve temperature was increased. For 1050 psi backing pressure and  $-160^\circ\text{C}$  valve temperature, the average cluster radius 1 mm above the 150  $\mu\text{m}$  orifice was  $\sim 1.8$  nm. At  $-140^\circ\text{C}$ , the cluster radius dropped to  $\sim 0.5$  nm for the same backing pressure. Above  $-140^\circ\text{C}$ , the cluster size was below the 0.5 nm measurement threshold.

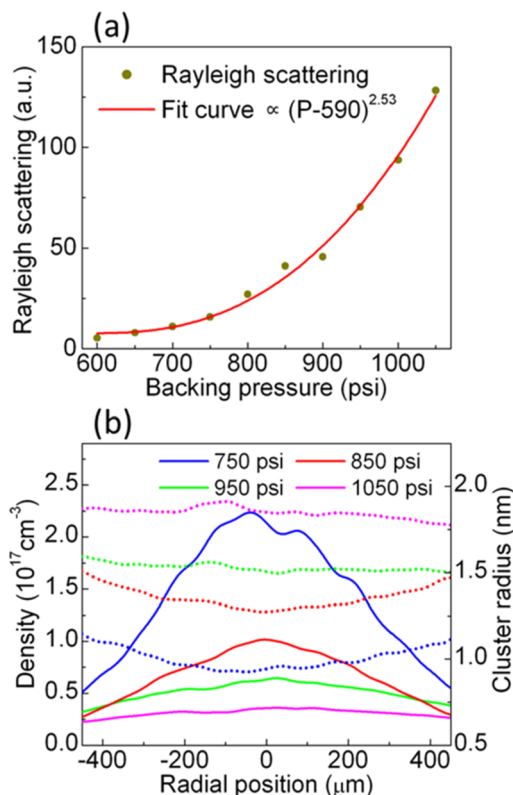


**FIG. 7.** Rayleigh scatter signal vs backing pressure (a) and cluster density (solid line) and size (dotted line) at a height  $\sim 1$  mm above the 150  $\mu\text{m}$  nozzle (b) with the jet reservoir held at  $-160^\circ\text{C}$ .

## VI. CONCLUSIONS

The development of thin, high density gas jet targets for near critical laser-plasma interaction experiments with Ti:sapphire laser systems has thus far been limited to a few approaches. In this paper, a jet design based on a cryogenically cooled pulsed solenoid valve was described. The jet was shown to be capable of reaching hydrogen molecule densities as high as  $9 \times 10^{20} \text{ cm}^{-3}$  in a  $\sim 200 \mu\text{m}$  FWHM Gaussian density profile when the jet was backed with 1000 psi and cooled to  $-160^\circ\text{C}$ . When fully ionized, this brings the peak plasma density above the (nonrelativistic) critical density for Ti:sapphire lasers, making this jet an interesting target for electron and ion acceleration experiments.

Estimates of the output density scaling with valve backing pressure and temperature were made by modeling the gas flow through the nozzle as steady and isentropic. Reaching the highest density output possible was found to require a sonic nozzle design, with the output molecular density directly proportional to the density within the valve reservoir. The equation of state prediction, that gas density at the nozzle exit scales as  $T_0^{-1}$ , is borne out by our measurements of cryogenically cooled jets, which yield a density scaling of  $T_0^{-0.87}$ .

Rayleigh scattering measurements showed that clustering of the high density gas occurs only  $\sim 500 \mu\text{m}$  and farther above the nozzle orifice. Average hydrogen cluster radii of  $\sim 1$  nm were measured approximately 1 mm above the nozzle for the highest backing pressures and lowest reservoir temperatures. The cluster size measurements show that clustering is negligible in experiments operating near the nozzle exit plane where the gas density is highest.

## ACKNOWLEDGMENTS

We thank George Hine, Yan Tay, and Kiyong Kim for technical discussions and assistance. This work was supported by the U.S. Department of Energy (Grant No. DESC0019735), the National Science Foundation (Grant No. PHY1619582), the Department of Homeland Security (Grant No. 2016DN077ARI104), and the Defense Threat Reduction Agency (Grant No. HDTRA11510002).

## REFERENCES

- C. G. R. Geddes, C. Toth, J. van Tilborg, E. Esarey, C. B. Schroeder, D. Bruhwiler, C. Nieter, J. Cary, and W. P. Leemans, *Nature* **431**, 538 (2004).
- Y. Fukuda, A. Y. Faenov, M. Tampo, T. A. Pikuz, T. Nakamura, M. Kando, Y. Hayashi, A. Yogo, H. Sakaki, T. Kameshima, A. S. Pirozhkov, K. Ogura, M. Mori, T. Z. Esirkepov, J. Koga, A. S. Boldarev, V. A. Gasilov, A. I. Magunov, T. Yamauchi, R. Kodama, P. R. Bolton, Y. Kato, T. Tajima, H. Daido, and S. V. Bulanov, *Phys. Rev. Lett.* **103**, 165002 (2009).
- A. Lifschitz, F. Sylla, S. Kahaly, A. Flacco, M. Veltcheva, G. Sanchez-Arriaga, E. Lefebvre, and V. Malka, *New J. Phys.* **16**, 033031 (2014).
- C. Gahn, G. D. Tsakiris, A. Pukhov, J. Meyer-Ter-Vehn, G. Pretzler, P. Thirolf, D. Habs, and K. J. Witte, *Phys. Rev. Lett.* **83**, 4772 (1999).
- A. Willner, F. Tavella, M. Yeung, T. Dzelzainis, C. Kamperidis, M. Bakarezos, D. Adams, M. Schulz, R. Riedel, M. C. Hoffmann, W. Hu, J. Rossbach, M. Drescher, N. A. Papadogiannis, M. Tatarakis, B. Dromey, and M. Zepf, *Phys. Rev. Lett.* **107**, 175002 (2011).
- C. Altucci, C. Beneduce, R. Bruzzese, C. De Lisio, G. S. Sorrentino, T. Starczewski, and F. Vigilante, *J. Phys. D: Appl. Phys.* **29**, 68 (1999).
- A. Depresseux, E. Oliva, J. Gautier, F. Tissandier, G. Lambert, B. Vodungbo, J.-P. P. Goddet, A. Tafzi, J. Nejd, M. Kozlova, G. Maynard, H. T. Kim,

- K. T. Phuoc, A. Rousse, P. Zeitoun, S. Sebban, K. Ta Phuoc, A. Rousse, P. Zeitoun, and S. Sebban, *Phys. Rev. Lett.* **115**, 083901 (2015).
- <sup>8</sup>T. Ditmire, J. Zweiback, V. P. Yanovsky, T. E. Cowan, G. Hays, and K. B. Wharton, *Nature* **398**, 489 (1999).
- <sup>9</sup>M. Krishnan, K. W. Elliott, C. G. R. Geddes, R. A. van Mourik, W. P. Leemans, H. Murphy, and M. Clover, *Phys. Rev. Spec. Top.—Accel. Beams* **14**, 033502 (2011).
- <sup>10</sup>F. Sylla, M. Veltcheva, S. Kahaly, A. Flacco, and V. Malka, *Rev. Sci. Instrum.* **83**, 033507 (2012).
- <sup>11</sup>E. Parra, S. J. McNaught, and H. M. Milchberg, *Rev. Sci. Instrum.* **73**, 468 (2002).
- <sup>12</sup>S. Semushin and V. Malka, *Rev. Sci. Instrum.* **72**, 2961 (2001).
- <sup>13</sup>R. Azambuja, M. Eloy, G. Figueira, and D. Neely, *J. Phys. D: Appl. Phys.* **32**, L35 (1999).
- <sup>14</sup>A. Murakami, J. Miyazawa, H. Tsuchiya, T. Murase, N. Ashikawa, T. Morisaki, R. Sakamoto, and H. Yamada, *J. Plasma Fusion Res. Ser.* **9**, 79 (2010).
- <sup>15</sup>J. Fan, T. R. Clark, and H. M. Milchberg, *Appl. Phys. Lett.* **73**, 3064 (1998).
- <sup>16</sup>D. Kaganovich, M. H. Helle, D. F. Gordon, and A. Ting, *Phys. Plasmas* **18**, 120701 (2011).
- <sup>17</sup>A. Buck, J. Wenz, J. Xu, K. Khrennikov, K. Schmid, M. Heigoldt, J. M. Mikhailova, M. Geissler, B. Shen, F. Krausz, S. Karsch, and L. Veisz, *Phys. Rev. Lett.* **110**, 185006 (2013).
- <sup>18</sup>B. D. Layer, A. G. York, S. Varma, Y.-H. Chen, and H. M. Milchberg, *Opt. Express* **17**, 4263 (2009).
- <sup>19</sup>S. J. Yoon, A. J. Goers, G. A. Hine, J. D. Magill, J. A. Elle, Y.-H. Chen, and H. M. Milchberg, *Opt. Express* **21**, 15878 (2013).
- <sup>20</sup>A. J. Goers, G. A. Hine, L. Feder, B. Miao, F. Salehi, J. K. Wahlstrand, and H. M. Milchberg, *Phys. Rev. Lett.* **115**, 194802 (2015).
- <sup>21</sup>T. Nakamura, S. V. Bulanov, T. Z. Esirkepov, and M. Kando, *Phys. Rev. Lett.* **105**, 135002 (2010).
- <sup>22</sup>D. Haberberger, S. Tochitsky, F. Fiuza, C. Gong, R. A. Fonseca, L. O. Silva, W. B. Mori, and C. Joshi, *Nat. Phys.* **8**, 95 (2012).
- <sup>23</sup>F. Salehi, A. J. Goers, G. A. Hine, L. Feder, D. Kuk, B. Miao, D. Woodbury, K. Y. Kim, and H. M. Milchberg, *Opt. Lett.* **42**, 215 (2017).
- <sup>24</sup>F. Salehi, *High Repetition Rate Laser-Driven Electron Acceleration to Mega-Electron-Volt Energies* (University of Maryland College Park, 2019).
- <sup>25</sup>I. Prencipe, J. Fuchs, S. Pascarelli, D. W. Schumacher, R. B. Stephens, N. B. Alexander, R. Briggs, M. Büscher, M. O. Cernaianu, A. Choukourov, M. De Marco, A. Erbe, J. Fassbender, G. Fiquet, P. Fitzsimmons, C. Gheorghiu, J. Hund, L. G. Huang, M. Harmand, N. J. Hartley, A. Irman, T. Kluge, Z. Konopkova, S. Kraft, D. Kraus, V. Leca, D. Margarone, J. Metzkes, K. Nagai, W. Nazarov, P. Lutoslawski, D. Papp, M. Passoni, A. Pelka, J. P. Perin, J. Schulz, M. Smid, C. Spindloe, S. Steinke, R. Torchio, C. Vass, T. Wiste, R. Zaffino, K. Zeil, T. Tschentscher, U. Schramm, and T. E. Cowan, *High Power Laser Sci. Eng.* **5**, e17 (2017).
- <sup>26</sup>K. M. George, J. T. Morrison, S. Feister, G. Ngirmang, J. R. Smith, A. J. Klim, J. Snyder, D. Austin, W. Erbsen, K. D. Frische, J. Nees, C. Orban, E. A. Chowdhury, and W. M. Roquemore, *High Power Laser Sci. Eng.* **7**, e50 (2019).
- <sup>27</sup>S. Feister, D. R. Austin, J. T. Morrison, K. D. Frische, C. Orban, G. Ngirmang, A. Handler, J. R. H. Smith, M. Schillaci, J. A. LaVerne, E. A. Chowdhury, R. R. Freeman, and W. M. Roquemore, *Opt. Express* **25**, 18736 (2017).
- <sup>28</sup>M. Gauthier, C. B. Curry, S. Göde, F.-E. Brack, J. B. Kim, M. J. Macdonald, J. Metzkes, L. Obst, M. Rehwald, C. Rödel, H.-P. Schlenvoigt, W. Schumaker, U. Schramm, K. Zeil, and S. H. Glenzer, *Appl. Phys. Lett.* **111**, 114102 (2017).
- <sup>29</sup>L. Obst, S. Göde, M. Rehwald, F. E. Brack, J. Branco, S. Bock, M. Bussmann, T. E. Cowan, C. B. Curry, F. Fiuza, M. Gauthier, R. Gebhardt, U. Helbig, A. Huebl, U. Hübner, A. Irman, L. Kazak, J. B. Kim, T. Kluge, S. Kraft, M. Loeser, J. Metzkes, R. Mishra, C. Rödel, H. P. Schlenvoigt, M. Siebold, J. Tiggesbäumker, S. Wolter, T. Ziegler, U. Schramm, S. H. Glenzer, and K. Zeil, *Sci. Rep.* **7**, 10248 (2017).
- <sup>30</sup>D. Margarone, A. Velyhan, J. Dostal, J. Ullschmied, J. P. Perin, D. Chatain, S. Garcia, P. Bonnay, T. Pisarczyk, R. Dudzak, M. Rosinski, J. Krasa, L. Giuffrida, J. Prokupek, V. Scuderi, J. Psikal, M. Kucharik, M. De Marco, J. Cikhardt, E. Krousky, Z. Kalinowska, T. Chodukowski, G. A. P. Cirrone, and G. Korn, *Phys. Rev. X* **6**, 041030 (2016).
- <sup>31</sup>J. T. Morrison, S. Feister, K. D. Frische, D. R. Austin, G. K. Ngirmang, N. R. Murphy, C. Orban, E. A. Chowdhury, and W. M. Roquemore, *New J. Phys.* **20**, 069501 (2018).
- <sup>32</sup>A. J. Goers, *Electron Acceleration by Femtosecond Laser Interaction with Micro-Structured Plasmas* (University of Maryland College Park, 2015).
- <sup>33</sup>U. Even, *EPJ Tech. Instrum.* **2**, 17 (2015).
- <sup>34</sup>K. Schmid and L. Veisz, *Rev. Sci. Instrum.* **83**, 053304 (2012).
- <sup>35</sup>D. Atkinson and M. Smith, *Rev. Sci. Instrum.* **66**, 4434 (1995).
- <sup>36</sup>N. Lemos, N. Lopes, J. M. Dias, and F. Viola, *Rev. Sci. Instrum.* **80**, 103301 (2009).
- <sup>37</sup>P. M. Gerhart, R. J. Gross, and J. I. Hochstein, *Fundamentals of Fluid Mechanics* (Addison-Wesley, 1992).
- <sup>38</sup>P. H. Oosthuizen and W. E. Carscallen, *Compressible Fluid Flow* (McGraw-Hill, 1997).
- <sup>39</sup>S. P. Nikitin, T. M. Antonsen, T. R. Clark, Y. Li, and H. M. Milchberg, *Opt. Lett.* **22**, 1787 (1997).
- <sup>40</sup>K. Y. Kim, V. Kumarappan, and H. M. Milchberg, *Appl. Phys. Lett.* **83**, 3210 (2003).
- <sup>41</sup>M. Takeda, H. Ina, and S. Kobayashi, *J. Opt. Soc. Am.* **72**, 156 (1982).
- <sup>42</sup>T. M. Miller and B. Bederson, *Adv. At. Mol. Phys.* **13**, 1 (1978).
- <sup>43</sup>M. Kalal and K. A. Nugent, *Appl. Opt.* **27**, 1956 (1988).
- <sup>44</sup>B. R. Munson, D. F. Young, and T. H. Okiishi, *Fundamentals of Fluid Mechanics*, 2nd ed. (John Wiley & Sons, 1997).
- <sup>45</sup>H. M. Milchberg, K. Y. Kim, V. Kumarappan, B. D. Layer, and H. Sheng, *Philos. Trans. R. Soc., A* **364**, 647 (2006).
- <sup>46</sup>T. Ditmire, T. Donnelly, R. W. Falcone, and M. D. Perry, *Phys. Rev. Lett.* **75**, 3122 (1995).
- <sup>47</sup>Y. Fukuda, H. Sakaki, M. Kanasaki, A. Yogo, S. Jinno, M. Tampo, A. Y. Faenov, T. A. Pikuz, Y. Hayashi, M. Kando, A. S. Pirozhkov, T. Shimomura, H. Kiriya, S. Kurashima, T. Kamiya, K. Oda, T. Yamauchi, K. Kondo, and S. V. Bulanov, *Radiat. Meas.* **50**, 92 (2013).
- <sup>48</sup>L. M. Chen, J. J. Park, K. H. Hong, J. L. Kim, J. Zhang, and C. H. Nam, *Phys. Rev. E* **66**, 025402 (2002).
- <sup>49</sup>Y. L. Shao, T. Ditmire, J. W. G. Tisch, E. Springate, J. P. Marangos, and M. H. R. Hutchinson, *Phys. Rev. Lett.* **77**, 3343 (1996).
- <sup>50</sup>T. Caillaud, F. Blasco, F. Dorchies, Y. Glinec, C. Stenz, and J. Stevefelt, *Nucl. Instrum. Methods Phys. Res., Sect. B* **205**, 329 (2003).
- <sup>51</sup>T. Ditmire, J. Zweiback, V. P. Yanovsky, T. E. Cowan, G. Hays, and K. B. Wharton, *Phys. Plasmas* **7**, 1993 (2000).